Heteroepitaxy of β-$FeSi_2$ on Si by gas-source MBE

A. Rizzi,* B.N.E. Rösen, D. Freundt, Ch. Dieker, and H. Lüth
Institut für Schicht- und Ionentechnik, Forschungszentrum Jülich, D-52425 Jülich, Germany

D. Gerthsen
Laboratorium für Elektronenmikroskopie, Universität Karlsruhe, Kaiserstrasse 12, D-76128 Karlsruhe, Germany
(Received 17 November 1994)

The gas-source molecular-beam epitaxy (GSMBE) of β-$FeSi_2$ layers on Si(111) and Si(001) has been studied. Results from two different growth processes, depending on the choice of either SiH_4 or Si_2H_6 as the silicon gas source, are discussed. $Fe(CO)_5$ acts as the Fe source for the silicide growth in both processes. Concerning surface roughness, thickness uniformity, and substrate/overlayer interface sharpness, best growth temperatures are found to be from 450 to 550 °C for both the SiH_4 and Si_2H_6 GSMBE processes. *In situ* electron spectroscopy combined with transmission-electron-microscopy structural analysis allows the identification of the grown silicide phases; furthermore, a heavily p-type doped accumulation layer is found to form at the surface, as revealed by high-resolution electron-energy-loss-spectroscopy. High defect optical absorption is measured below the edge region ($E_g \sim 0.87$ eV) and compared with common semiconductor materials. The RT electrical properties as measured by Hall effect are shown to be masked by a contribution from the substrate. At 77 K the mobility and carrier concentration of the grown β-$FeSi_2$ layers are $\mu \sim 2$ cm^2/V s and $p \sim 2 \times 10^{18}$ cm^{-3}, respectively.

I. INTRODUCTION

The semiconducting phase of iron disilicide, β-$FeSi_2$, has attracted considerable interest in the last few years because it could open new possibilities for other silicon-based heterostructures besides the Si-Ge alloy system to be of interest for optoelectronics and microelectronics.

Heteroepitaxy of thin β-$FeSi_2$ layers on both (111) and (001) silicon surfaces has been achieved by different techniques mainly under ultrahigh vacuum (UHV) conditions and it has turned out to be a difficult concern.[1–3] The complex orthorhombic structure of β-$FeSi_2$ intrinsically causes the growth of differently oriented epitaxial domains on both types of silicon surfaces. Furthermore, depending on the growth technique and conditions, different epitaxial relations with the substrate are observed, which all have a relatively large lattice mismatch to silicon.

In the case of very thin layers a better matched epitaxial interface has been shown to induce the formation of pseudomorphic metallic phases that do not occur in the equilibrium bulk phase diagram.[4–6] The temperature-induced phase transition towards the equilibrium β-$FeSi_2$ phase has been studied and different paths have been observed, depending on the growth technique.

Besides their interesting fundamental character, these studies aim at investigating the potential role of β-$FeSi_2$ as a material for applications in silicon-based optoelectronics and microelectronics. The measured direct energy gap of about 0.87 eV (~ 1.43 μm) matches very well with the optimum transmission window of optical fibers. However, recent experimental optical results agree with the theoretical prediction of an absolute indirect gap for the β-$FeSi_2$ very close in energy to the direct one.[7–9] These findings would prevent the use of the material in Si-based optoelectronic applications as a light emitter; at present the Si-Ge system and porous silicon seem to be more promising in that field. Nevertheless other possible applications, e.g., as infrared detector or for use in thin film solar cell technology still motivate further investigation.

In this work we report on a study performed on the growth by gas-source molecular-beam epitaxy (GSMBE) and characterization of β-$FeSi_2$/Si heterostructures.

Gas-source MBE (also known as chemical beam epitaxy, CBE) has become a widely used technique for the deposition of semiconductor materials. The reactant gases are delivered as molecular beams with no gas-phase reaction prior to reactant adsorption. In contrast to MBE, the gaseous sources do not have to be heated significantly above RT, thus avoiding the presence of hot surfaces in the vicinity of the sample. They ensure continuous performance and the UHV growth environment allows, as in MBE, a high control of the growth process *in situ*. Furthermore, the possibility of selective growth onto a silicon dioxide patterned substrate is very attractive. $FeSi_2$ layers have been grown on Si(111) and Si(001) substrates. A comparison between two different growth processes, depending on the choice of either SiH_4 or Si_2H_6 as silicon gas source, is reported. $Fe(CO)_5$ provides the Fe component for the silicide growth in both processes.

In situ low-energy electron diffraction (LEED) displays the surface symmetry of the grown silicide layers that reflects the overlayer crystal symmetry and its epitaxial relation to the substrate. A more complete structural analysis is then achieved by means of transmission electron microscopy (TEM), which reveals details of the sample

0163-1829/95/51(24)/17780(15)/$06.00

crystal structure and morphology of the bulk of the layer on a scale ranging from several micrometers down to the atomic scale. Information about the chemical composition and crystalline quality of the grown heterostructures is also gained by Rutherford backscattering (RBS) analysis. The electronic and vibrational properties of the iron silicide layers grown are investigated by *in situ* high-resolution electron-energy-loss spectroscopy (HREELS). The incoming electrons are scattered due to charge density fluctuations in the crystal that can be caused by, e.g., excitations of phonons, surface plasmons, or single particle excitations (intraband and interband electronic transitions). The energy-loss spectra measured in reflection geometry (dipole scattering regime) thus give a picture of the crystal surface elementary excitations. Electronic valence band spectra are measured by means of ultraviolet photoemission spectroscopy (UPS) and their features allow the identification of the grown silicide phase.

II. EXPERIMENT

The UHV system consists of a GSMBE growth chamber connected with two analysis chambers for the *in situ* characterization. The first analysis chamber is equipped with a three-grid LEED system and a HREELS spectrometer with two stage monochromator and analyzer. Photoelectron spectroscopy is performed in the second analysis chamber. A He discharge lamp ($\hbar\omega = 21.2$ eV) serves as ultraviolet source and for the x-ray excited spectra monochromatized Al K_α radiation ($\hbar\omega = 1486.8$ eV) is used. The base pressure is $\sim 2\times10^{-11}$ Torr in the growth and in the first analysis chamber, $\sim 2\times10^{-10}$ Torr in the photoemission system. A load-lock entry allows a rapid insertion of the samples into the growth unit.

High resistivity ($\rho \sim 5000\ \Omega$cm) Si(111) and Si(001) wafers (6×15 mm^2) are used as substrates. They are wet chemically treated *ex situ* by a modified Shiraki method, which leaves a thin oxide layer on the sample surface. Complete desorption of this oxide layer is achieved in UHV after annealing at 820 °C for about 15 min resulting in a clean Si(111)(7×7) or Si(001)(2×1) reconstructed surface as checked by LEED and HREELS.

Either silane (SiH_4) or disilane (Si_2H_6) are used as silicon gas sources for the two different investigated GSMBE processes. Iron pentacarbonyl, $Fe(CO)_5$, serves as iron gas source in both cases. Each gas is injected into the chamber separately and focused onto the heated silicon substrate, placed a distance of 6 cm from the gas line outlets. The gas flow is controlled by Baratron valves. In order to get a homogeneous flow profile at the sample the gas lines are equipped with glass capillary arrays, whose pore diameter is 50 μm. The gas pressure p_i at the inlet leak valves is of the order of 10^{-2} Torr and the background pressure p_b in the chamber during the growth is of the order of 10^{-6} Torr. The partial pressure of the two components at the crystal surface depends on the pressure at each inlet leak valve, which in turn is directly related to the background pressure in the growth chamber. A calibration of the gas inlet system gives for $p_i = 1\times10^{-2}$ Torr the following partial pressures at the crystal surface: $p_{SiH_4} = p_b/0.018 = 0.6\times10^{-4}$ Torr and $p_{Fe(CO)_5} = p_b/0.0075 = 1.3\times10^{-4}$ Torr. At the beginning of each GSMBE growth process the substrate temperature is set up, then the Si source is opened first and after 1 min the iron source is switched on. At the end the Fe line is closed, leaving the Si line still open for 1 min. Finally the sample temperature is lowered at a rate of -1 K/s to RT before the sample is transferred into the analysis system. Within the sensitivity of the *in situ* characterization methods employed no traces of carbon or oxygen incorporation in the silicide films are observed.

III. GROWTH PROCESS WITH SiH_4

The first series of growth studies are concerned with the effect of a systematic variation of the Si-to-Fe composition ratio at the growing surface. A sequence of silicide layers is grown on Si(001) in the range from 0:1 up to 5:1 Si:Fe atomic ratio. The growth temperature is 550 °C and the deposition time is 3 h for each process. The silicide phase formed is the semiconducting β-$FeSi_2$ for all samples, as revealed by the presence of the Fuchs-Kliewer phonons in the HREELS spectra and the shape of the UPS spectra with negligible intensity at the Fermi level.[10]

A scanning-electron-microscopy (SEM) analysis (not reported here) shows very different surface morphologies for the different Si:Fe ratios.[9] High roughness is observed if only Fe impinges upon the surface and with increasing Si feed the roughness decreases. The smoothest surfaces, on a scale of 0.1 μm, are achieved by equal Fe and Si gas pressures or slight Si overpressure. A too high Si gas feed induces three-dimensional (3D) growth with island formation.

In order to determine the growth rate a series of β-$FeSi_2$ films has been grown on Si(111) and Si(001) with varying deposition times at a substrate temperature of 550 °C. The beam gas pressures are 2.5×10^{-4} Torr and 3×10^{-4} Torr for $Fe(CO)_5$ and SiH_4, respectively. Due to these relatively low values, gas-phase collisions can be ignored when considering the growth kinetics and therefore only surface reactions are assumed to be important. The layer thickness increases linearly with the deposition time as determined via RBS. On Si(111) and Si(001) growth rates of about 2 Å/min and 2.5 Å/min are obtained.

Figure 1 shows the Arrhenius plot of the growth rate r for the β-$FeSi_2$ growth on Si(111) and Si(001). Data from Si(001) homoepitaxy with SiH_4 by Hirose *et al.*[11] are also shown; the SiH_4 pressure in their GSMBE process is 2×10^{-4} Torr. The β-$FeSi_2$ growth rate as a function of the temperature shows a clear break: below $T = 600$ °C it does not significantly depend on the temperature, while at higher T a thermally activated behavior is observed. In the whole temperature range a slightly higher growth rate is achieved on Si(001) than on Si(111). A break at almost the same temperature is also found for the silicon growth process. A relation between the two

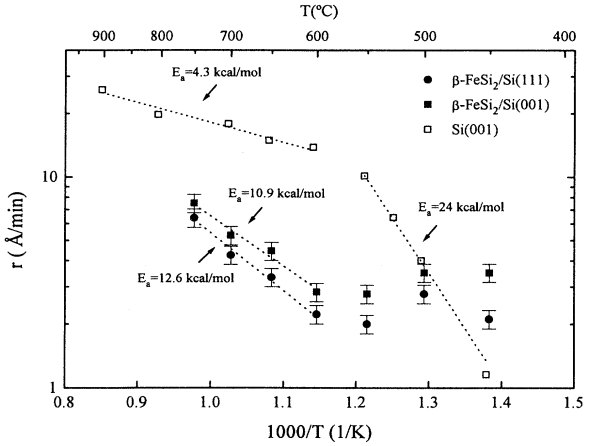

FIG. 1. β-$FeSi_2$ growth rate on Si(111) and Si(001) as a function of the substrate temperature. The gas pressures are 2.5×10^{-4} and 3×10^{-4} Torr for $Fe(CO)_5$ and SiH_4, respectively. Each sample was grown at the selected growth temperature for 3 h. The growth rate is derived from the measured thickness by RBS with an estimated relative error of 10%.

processes might be inferred even though the growth rate temperature dependence above and below this breaking point is different for silicon homoepitaxy and for the silicide growth. It is therefore useful for the discussion to recall briefly the Si growth model generally proposed in the literature.[12,13]

The growth model for silicon homoepitaxy with silane considers adsorption of SiH_4 followed by diffusion and incorporation in a sequential manner. The net reaction is

$$SiH_4(g) \Rightarrow Si(s) + 2H_2(g) \quad .$$

Two different growth mechanisms with different activation energies are identified, depending on the growth limiting process. An adsorption-limited process occurs on a sparsely covered silicon surface, when the hydrogen surface coverage is low and therefore adsorption site availability is high (high temperature limit). Silicon carrying fragments are presumed to diffuse fast towards the atomic edge steps to specific sites where incorporation occurs. This process is characterized by a low overall activation energy ($\sim$ 4 kcal/mol). In a high surface coverage regime attained in the low temperature limit, an increase in the overall activation energy is observed as the SiH_4 adsorption rate is controlled by the rate of H_2 desorption, producing dangling bonds.

Concerning the iron gas source it is known that $Fe(CO)_5$ shows a relatively low activation energy ($\sim$ 6.2 kcal/mol) for the thermal decomposition reaction on a Si(001) surface in UHV,

$$Fe(CO)_5(g) \Rightarrow Fe_{ads} + 5CO(g) \ .$$

Surface-to-bulk transport of iron is observed to start above 400 °C and the diffusion kinetic of Fe in Si is characterized by an activation energy of 16 kcal/mol.[14]

Referring now back to the temperature dependence of the silicide growth rate reported in Fig. 1, it can then be expected that the lower temperature region in this case is also characterized by a high-coverage regime. The presence of activated iron, cobalt, and nickel is generally known to catalyze the synthesis of saturated (C_nH_{2n+2}) and unsaturated (C_nH_{2n}) aliphatic hydrocarbons from carbon monoxide and hydrogen.[15] An example of this commercially important Fischer-Tropsch synthesis is

$$CO + 3H_2 \Rightarrow CH_4 + H_2O(g) + 49.26 \text{ kcal}$$

and this reaction runs already at 250–300 °C due to the catalytic effect of, e.g., nickel. This kind of exothermic reaction might thus explain the observed temperature independent growth rate that characterizes the growth of the iron disilicide by codeposition in the lower temperature range. Above 600 °C, when in the Si growth the adsorption of silane becomes the limiting process, the transition towards a low-coverage surface slows down the reaction between Fe and Si at the surface and the fast diffusion of Fe in the substrate becomes the important growth mechanism.[14] This also explains the increase in the overall roughness observed for the samples grown at higher temperatures.

Further evidence for the reaction of the Fe with the Si substrate at higher growth temperatures is provided by growing the silicide on a SiO_2 patterned Si substrate. A cross-section TEM picture of a sample grown at 700 °C is shown in Fig. 2. The plane of the picture lies perpendicular to the 1 μm wide oxide strips; the original silicon substrate surface is marked by the Si/SiO_2 interface in the middle of the image. The β-$FeSi_2$ is found to grow selectively on the bare silicon surface (left and right of the SiO_2) and it is clearly seen that a significant layer fraction has grown by diffusion into the substrate.

Figure 3 shows cross-section images of β-$FeSi_2$ layers grown by GSMBE at 550 °C substrate temperature on Si(111) and Si(001), respectively. A smooth surface and a sharp interface are observed for the epitaxy on the Si(111) substrate, while epitaxy on Si(001) results in a slightly higher surface and interface roughness. The different contrast within the grown layers arises from silicide grains with different azimuthal orientations. Strain contrast is also clearly seen at the interface on the silicon

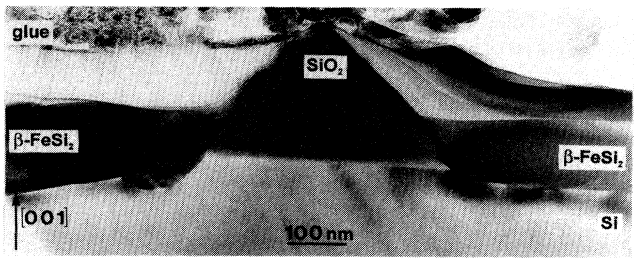

FIG. 2. Cross-section TEM image showing the growth of β-$FeSi_2$ on a SiO_2 patterned Si(001) substrate. Growth temperature is 700 °C.

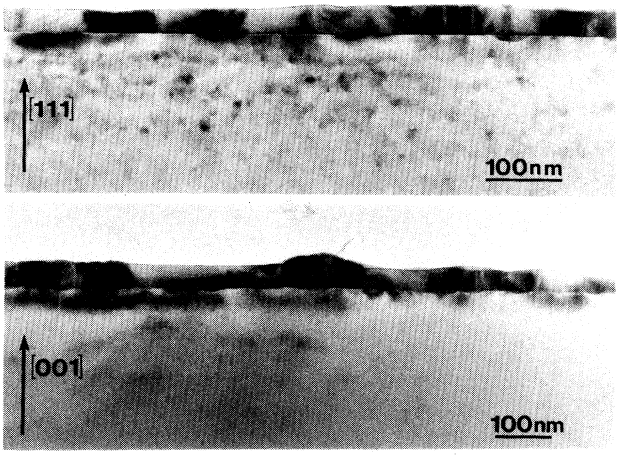

FIG. 3. Cross-section TEM images of β-$FeSi_2$ layers grown on Si(111) (top) and Si(001) (bottom). Growth temperature is 550 °C and growth time 3 h.

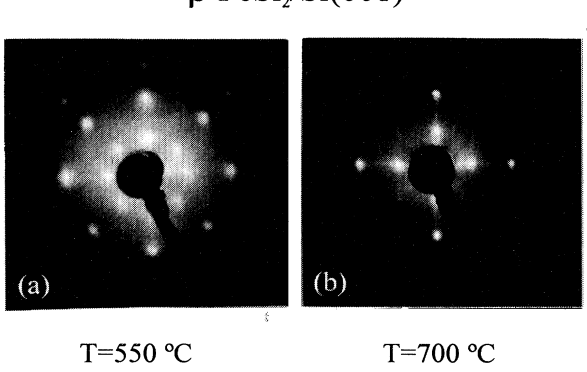

FIG. 4. 63 eV LEED pattern of epitaxial β-$FeSi_2$ grown on Si(001) at (a) 550 °C (d = 360 Å) and (b) 700 °C (d = 900 Å).

substrate side.

RBS analysis confirms the $FeSi_2$ composition of the layers grown in the whole temperature range. Simulations of the measured spectra, assuming the growth of a uniform silicide overlayer, also indicate the tendency towards increasing film roughness with increasing growth temperature. This effect is more important for the heteroepitaxy of β-$FeSi_2$ on Si(001) than on Si(111).

The reported results show that β-$FeSi_2$/Si heterostructures can be grown by GSMBE with SiH_4 and $Fe(CO)_5$ in a wide substrate temperature range. Concerning the morphology of the grown films, the best results are obtained on Si(111) substrates in the temperature range from 450 °C to 550 °C and with a slight silane partial oversupply at the sample. In the next section the microstructure and epitaxial relationships of the heterostructures grown will be discussed.

IV. MICROSTRUCTURE AND EPITAXIAL RELATIONSHIPS

Semiconducting β-$FeSi_2$ crystallizes in an orthorhombic lattice with a = 9.863 Å, b = 7.791 Å, c = 7.833 Å; the primitive cell contains 48 atoms, 16 Fe and 32 Si atoms.[16] Even though there is no simple structure matching with the cubic silicon substrate, several groups have demonstrated the epitaxial growth of β-$FeSi_2$ on Si(111) and Si(001).[1,2,5,6,17,18] Due to the reduction of the layer symmetry as compared with the cubic substrate, several equivalent azimuthal orientations are expected and have been indeed observed for the epitaxy of β-$FeSi_2$ on both silicon substrates.

A. β-$FeSi_2$/Si(001)

LEED pictures of β-$FeSi_2$ grown on Si(001) at 550 °C (a) and 700 °C (b) are shown in Fig. 4. The primary electron energy is 63 eV. Both patterns show the epitaxial relationship with β-$FeSi_2$(100)||Si(001). The azimuthal orientation shows differences at the two selected growth temperatures. At the higher temperature [Fig. 4(b)] one orientation is mainly observed; the lower temperature additionally induces a 45° rotated twofold symmetry pattern [Fig. 4(a)]. The two observed epitaxial relationships correspond to the two-dimensional real space configuration shown in Fig. 5. The Si(001) lattice points are plotted as small circles and the β-$FeSi_2$(100) unit cell by the dashed lines. The shaded areas describe the lattice unit cells. In one case the azimuthal orientation is β-$FeSi_2$[010]||Si⟨100⟩ with a linear mismatch of −4.3% and −3.8%; the other azimuthal orientation corresponds to β-$FeSi_2$[010]||Si⟨110⟩ with a linear mismatch of +1.5% and +2.0%. Similar results are reported for the growth

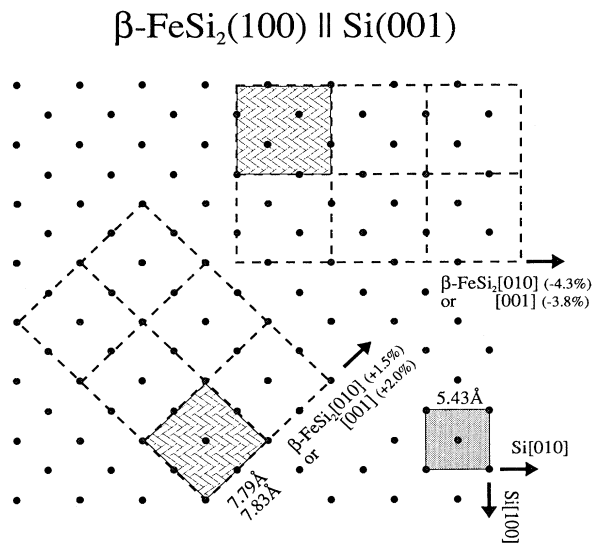

FIG. 5. Two-dimensional real space model for the epitaxy of β-$FeSi_2$ on Si(001). The plane of the figure corresponds to the Si(001) (circles) and β-$FeSi_2$(100) (dashed lines) lattice planes.

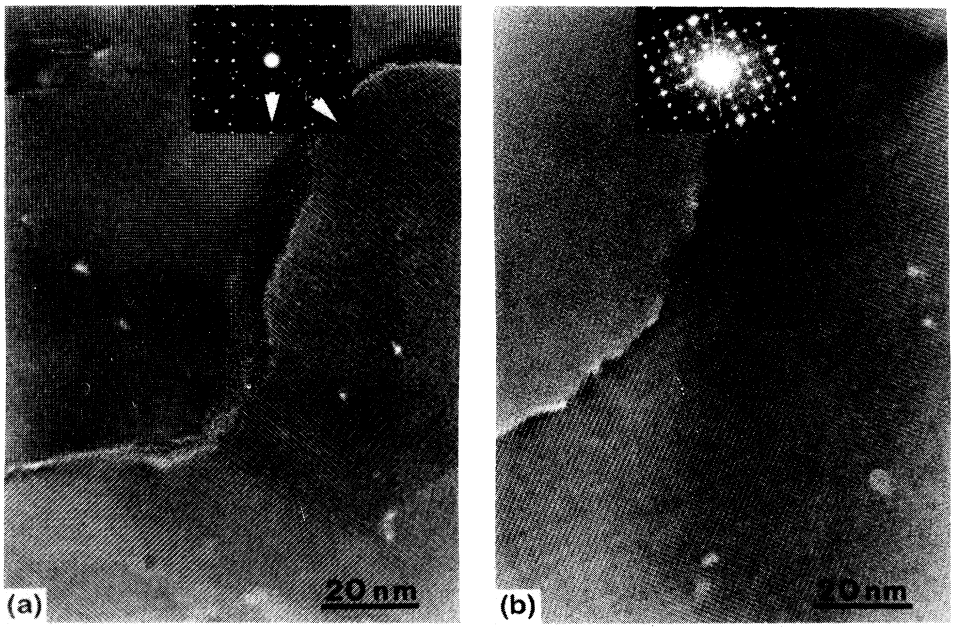

FIG. 6. HRTEM plan-view picture of β-$FeSi_2$(100) grown on Si(001) showing the boundary region between two epitaxial grains. (a) Grain boundary region of two domains rotated by 45°. (b) Grain boundary region of two domains that are only slightly tilted against each other. The lattice fringe resolution is reduced due to the tilt. The optical diffractograms of the boundary areas are inserted in the images.

by MBE.[1,17] In the GSMBE process not only the growth temperature affects the type of heteroepitaxy; a Si source oversupply is observed to induce preferentially both orientations in the whole temperature range.

A high-resolution plan-view TEM picture in the region of a grain boundary is shown in Fig. 6(a). The sample was grown by GSMBE at 550 °C. The (004) and (040) fringes of the β-$FeSi_2$ are clearly resolved that form an angle of 45° at the domain boundary thus confirming the results of the LEED investigation. The inserted selected area optical diffractogram was taken from both grains and shows the overlap of the two grain patterns that are rotated by 45° against each other. The directions of the reciprocal lattice vectors corresponding to the (010) planes in the two domains are marked by the arrows in the diffractogram. In other cases plan-view HRTEM reveals the formation of small-angle grain boundaries [Fig. 6(b)]. The inset shows the optical diffractogram of the two grains; the pattern of only one orientation is recognized. The loss of resolution in the grain on the right-hand side can be explained by a slight tilt of the [100] direction of the β-$FeSi_2$ with respect to the incident electron beam, which also gives rise to a broadening of the reflections in the optical diffractogram. The mean lateral size of the single epitaxial grains is in the order of 0.5 μm. RBS spectra taken on the present samples do not show any channeling in β-$FeSi_2$(100)/Si(001). Von Känel *et al.*,[1] however, have reported a minimum yield of 7.5% for MBE-grown β-$FeSi_2$(100)/Si(001). In their growth process a thin template silicide layer is formed at the substrate interface by low temperature deposition before proceeding with the MBE growth at 700 °C. This procedure should improve the silicide growth, mainly concerning the sharpness of the substrate interface. The GSMBE-grown β-$FeSi_2$ layers show a relatively rough interface to the substrate (Fig. 3) that might be the reason for the formation of epitaxial grains slightly tilted against each other. The described microstructure would of course prevent channeling effects in RBS.

In Fig. 7 a cross-section HRTEM image shows a region with two differently oriented grains. The insets display the optical diffractograms of the two grains. The left one shows the common epitaxial orientation β-$FeSi_2$(100)||Si(001). In the upper part of the right grain the β-$FeSi_2$(220) and β-$FeSi_2$(202) planes are clearly visible. The β-$FeSi_2$(202) planes are oriented almost parallel to one set of the {111} planes in the Si substrate, which corresponds to the epitaxial orientation commonly observed for β-$FeSi_2$ on Si(111) substrates. The interface roughness in this area most likely induces this epitaxial orientation.

B. β-$FeSi_2$/Si(111)

Similar to what is observed on Si(001), the epitaxy of iron disilicide on Si(111) also shows different epi-

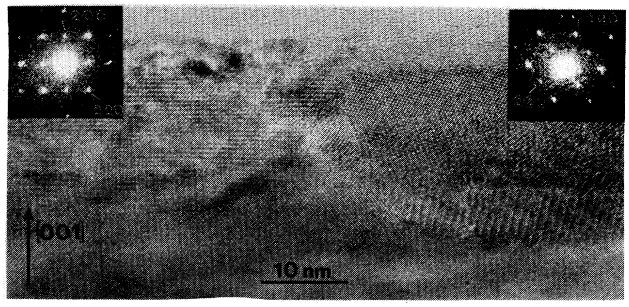

FIG. 7. Cross-section HRTEM image of two differently oriented grains (left and right) with the insets showing the optical diffractograms of the two regions. β-$FeSi_2$ was grown by GSMBE at 550 °C.

taxial relations in the lower and higher growth temperature range. Figure 8 displays the LEED patterns taken after GSMBE growth of β-$FeSi_2$ on Si(111) at three selected temperatures. As in the former case, the epitaxial relations are schematically shown in a two-dimensional real space model in Fig. 9. At 700 °C growth temperature [Fig. 8(c)] epitaxial grains of β-$FeSi_2$(101)/Si(111) or β-$FeSi_2$(110)/Si(111) are formed. Due to the small difference in the b and c lattice constants of the orthorhombic system, it is not possible to distinguish between the two possibilities in LEED experiments. The threefold rotational symmetry of the substrate induces the growth of three different azimuthal oriented domains, rotated by 120° against each other (Fig. 9, right-hand side). This is the most commonly observed epitaxial orientation for β-$FeSi_2$ grown on Si(111) by different growth methods and in particular the one first observed for solid-phase-epitaxy- (SPE) grown films.[19] Growth at 500 °C results in a different symmetry of the LEED pattern [Fig. 8(a)]. Twelve spots ordered in a ring geometry are recognized and they correspond to the growth of β-$FeSi_2$(100)||Si(111) with β-$FeSi_2$[010] or [001]||Si$\langle\bar{1}10\rangle$ (Fig. 9, left-hand side). The LEED pattern is composed of three equivalent azimuthal oriented domains, rotated by 120°. A mismatch of +1.4% (+2.0%) along Si$\langle\bar{1}10\rangle$ and of −1.9% (−2.4%) along Si$\langle\bar{1}\bar{1}2\rangle$ is calculated if a large common unit mesh is considered ($5b \times c$ or $5c \times b$). At 550 °C [Fig. 8(b)] an additional 12 spots, rotated by 15°, are identified and correspond to a different azimuthal orientation with respect to the substrate, β-$FeSi_2$[011]||Si$\langle\bar{1}01\rangle$ (Fig. 9, middle). Even though with lower intensity additional spots appear that correspond to the pattern observed at the higher temperature [Fig. 8(c)], i.e., β-$FeSi_2$(101)/Si(111) oriented grains. These results are confirmed by TEM; for a growth temperature of about 500 °C the grain sizes range from 50 nm to several μm.[20]

A minimum channeling yield of 57% in RBS spectra is measured for the β-$FeSi_2$ epitaxial layers grown at 450 °C; χ_{min} increases almost linearly up to a value of 86% by increasing the growth temperature up to 750 °C.

For the following discussion it must be recalled that the growth of different pseudomorphic $FeSi_2$ phases on Si(111), which do not exist as equilibrium bulk phases, has been reported in the literature.[1–6] Furthermore, even the metallic α-$FeSi_2$ phase, stable above 937 °C, has been observed to grow epitaxially on Si(111) in the temperature range 500 – 550 °C. It transforms into β-$FeSi_2$ either by annealing or during the growth, by increasing the layer thickness.[21–24]

In previous works we have shown that the β-$FeSi_2$ epitaxy on Si(111) by GSMBE with silane in the temperature range 450 – 550 °C is characterized by the formation of an epitaxial metallic γ-$FeSi_2$ layer at the interface with the silicon substrate.[2,20,25] The γ-$FeSi_2$ has a CaF_2 structure and is not stable in the bulk but it can be stabilized on Si(111) by an energetically favorable interface to the substrate. Interestingly the orthorhombic bulk structure, β-$FeSi_2$, arises by a slight distortion of the calcium fluorite lattice.[16,26]

Sirringhaus *et al.*[5] studied the $FeSi_2$/Si(111) epitaxy starting from a pseudomorphic $Fe_{0.5}\square_{0.5}Si$, with CsCl symmetry and a random occupation of 50% of the Fe sites. This $FeSi_2$ CsCl-derived defect phase can be grown by MBE on Si(111).[4,27] They found that the orientation of β-$FeSi_2$ formed after annealing is very much dependent on kinetic factors, in particular on the stoichiometry of the initial deposit. On the Si-rich or stoichiometric side β-$FeSi_2$(101) grains form, whereas on the Fe-rich side β-$FeSi_2$(100) and β-$FeSi_2$(001) grains are found to grow.

In the GSMBE process reported here different β-$FeSi_2$ orientations are observed as well and with increasing growth temperature there is a continuous change from β-$FeSi_2$(100) to β-$FeSi_2$(101). We do not have any evidence that a variation of the partial pressure ratio of the components induces a change in the orientation of the grown silicide. Actually, the transition among the different types of epitaxy relates to the growth temperature and occurs in the temperature region where the system exhibits a change in the growth mechanism, as discussed in Sec. III. In the diffusion controlled growth (high temperature range) the same orientation is obtained as in SPE; below 550 °C the codeposition from the gas phase is the major growth mechanism and the nucleation of β-$FeSi_2$(100) oriented grains is favored.

We believe that a determining factor in our process is

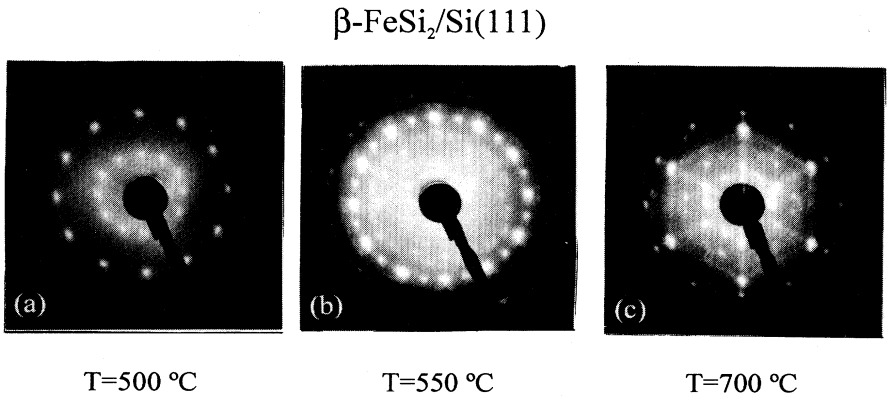

FIG. 8. LEED pattern of epitaxial β-$FeSi_2$ grown on Si(111) at (a) 500 °C (E = 46 eV, d = 500 Å), (b) 550 °C (E = 43 eV, d = 100 Å), and (c) 700 °C (E = 46 eV, d = 800 Å).

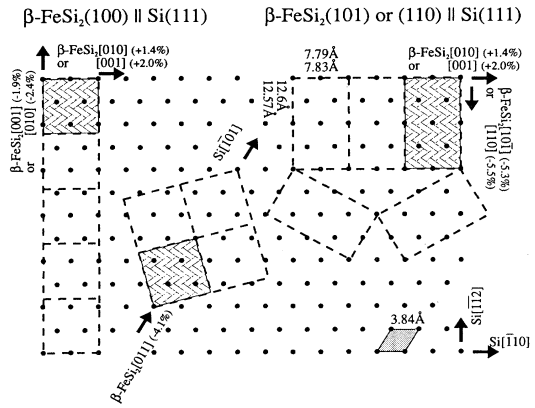

FIG. 9. Two-dimensional real space model for the epitaxy of β-$FeSi_2$ on Si(111). The plane of the figure corresponds to the Si(111) (circles) and on the left-hand side to β-$FeSi_2$(100) (dashed lines), on the right-hand side to β-$FeSi_2$(101) or β-$FeSi_2$(110) lattice planes.

the formation of a thin epitaxial γ-$FeSi_2$ layer between the Si(111) substrate and the semiconducting β phase in the lower temperature range. This has been shown by a combined *in situ* electron spectroscopy and HRTEM analysis.[20,25] In Fig. 10 a TEM cross-section image of the interface region along a ⟨112⟩-direction in the Si is shown. To confirm the presence of γ-$FeSi_2$, image simulations were carried out for Si and γ-$FeSi_2$ along the ⟨112⟩ projection. Details of the parameters entering the simulations are given elsewhere.[20] The projected crystal structures and the simulated images are inserted into

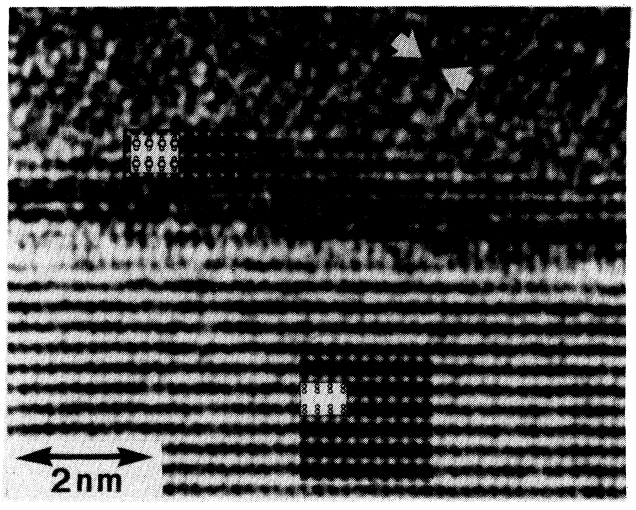

FIG. 10. High-resolution cross-section image with a Si⟨112⟩ zone axis oriented parallel to the electron beam. The interface region is shown with a thin γ-$FeSi_2$ layer [1–6 Si(111) layers] located between the substrate and the β-$FeSi_2$. The insets show simulations of the γ-$FeSi_2$ and the Si based on structural models also inserted in the figure (large circles Fe, small circles Si).

Fig. 10. The match between the experimental and simulated images is a strong indication of the presence of γ-$FeSi_2$ at the interface. The lattice parameter of the γ-$FeSi_2$ was $a = 5.389$ Å. Since the β-$FeSi_2$ is not oriented along a low index zone axis, only one set of lattice fringes corresponding to β-$FeSi_2$(202) is visible (indicated by the white arrows). The observed thickness variation of the γ-$FeSi_2$ interlayer in the range 1–6 monolayers is typical for a Stranski-Krastanov growth (islands on top of a two-dimensional layer). Linear muffin-tin orbital (LMTO) and full-potential linearized augmented-plane-wave method (FLAPW) calculations give equilibrium bulk lattice constants for the metastable γ-$FeSi_2$ of $a = 5.39$ Å (Ref. 26) and $a = 5.32$ Å (Ref. 28), respectively. The mismatch to the silicon substrate is therefore between 0.7% and 2%. The formation of islands in the growth of the thin γ-$FeSi_2$ layer provides a mechanism for the elastic relaxation of the lattice-parameter mismatch; when this is achieved, then the bulk stable β phase begins to grow. The thickness of the γ-$FeSi_2$ layer does not significantly increase when the growth temperature is lowered; therefore the presence of the layer is not related to a phase transformation of an originally thicker γ-$FeSi_2$ layer into β-$FeSi_2$. This also explains that the β phase growing on top does not necessarily have the orientation β-$FeSi_2$(101)||Si(111) expected when a γ film is transformed to the semiconducting β phase by a Jahn-Teller lattice distortion. The fact that the thin γ-$FeSi_2$ layer remains stabilized at the interface to the substrate can be due to a relevant energy gain from the bonding to the silicon substrate, as confirmed by total-energy semiempirical tight binding calculations.[29] In this way the γ layer provides an elastic buffer that accommodates the mismatch between the Si and the β-$FeSi_2$ without the need for misfit dislocations that has not been observed, either by plane-view or by cross-sectional TEM of layers up to 60 nm in thickness.

The results discussed so far show that the epitaxy of β-$FeSi_2$ on Si exhibits manifold aspects. The orthorhombic structure of the semiconducting phase is itself the major problem for the growth of monocrystalline layers on the cubic silicon. Depending on the Si surface symmetry, different azimuthal orientations are always obtained with a lateral size of the single grains that can be in the order of 1 μm. Furthermore, on the Si(111) surface metastable metallic $FeSi_2$ phases can grow due to the better matching to the substrate and the lower interface energy. Everything is very much dependent on the kinetics of the growth mechanism, which forces the system to grow in one orientation or the other with apparently no sharp transitions.

V. ELECTRONIC PROPERTIES

Figure 11 shows a sequence of UPS (a) and HREELS (b) spectra taken on a sample grown by GSMBE on a Si(111) substrate at $T = 450\,^{\circ}$C. The thickness of the $FeSi_2$ layer is 400 Å as measured by RBS. The bottom spectra are those of the clean silicon surface. After the epitaxial growth of $FeSi_2$ the top of the valence band

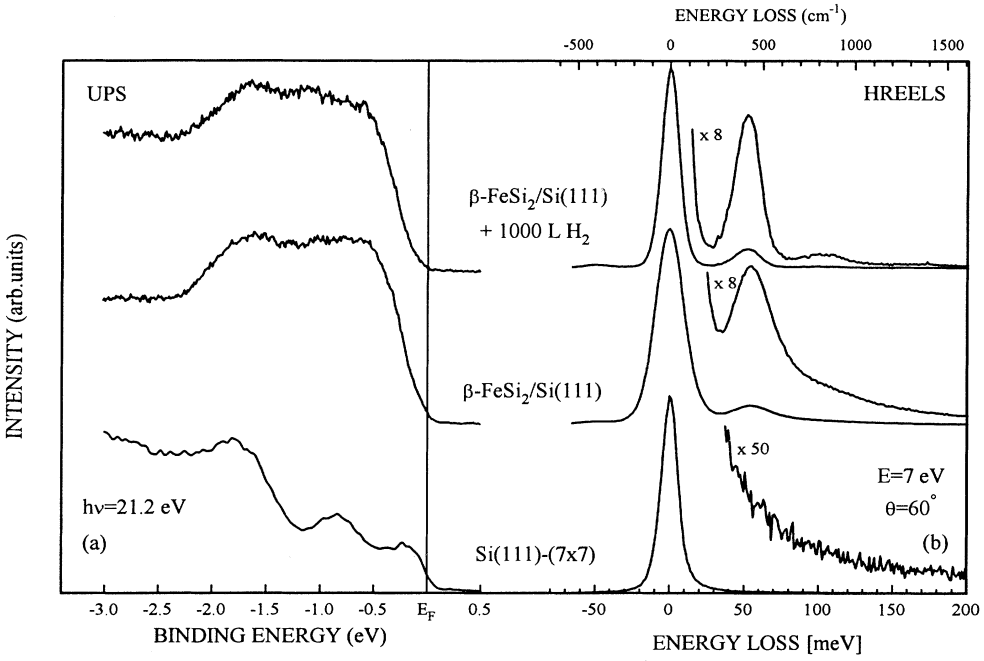

FIG. 11. UPS and HREELS spectra measured at room temperature, from the bottom to the top, on the clean Si(111)(7×7) surface, after the GSMBE of $FeSi_2$ at 450 °C (d = 400 Å) and after 1000 L hydrogen adsorption at RT (1 L = 10^{-6} Torr s). (a) Ultraviolet photoemission spectra. Photon energy is 21.2 eV, the Fermi level position is indicated by a vertical line at zero binding energy. (b) High-resolution electron-energy-loss spectra measured with a primary beam energy of 7 eV under specular reflection with 60° angle of incidence.

shows a rather broad distribution of occupied states centered at −1.2 eV binding energy and an extrapolated valence band maximum (VBM) at −80 meV. The elastic peak in the loss spectrum has clearly broadened, from 13.4 meV full width at half maximum (FWHM) at the clean surface up to 22.6 meV. An intense loss peak is measured at 50 meV superimposed on a continuous background extending up to 200 meV. After hydrogen adsorption at RT two main effects show up in the spectra. The top of the valence band mainly retains the same shape, but the VBM shifts to higher absolute binding energies at −200 meV. The elastic peak has narrowed down to 14 meV FWHM and consequently the broad loss continuum has reduced; the characteristic loss peak at 50 meV is now also revealed in its double loss excitation.

The well known (7 × 7) reconstruction of the Si(111) surface has metallic character and this is reflected by both measured spectra. The occupied density of states at the surface, as measured by UPS, shows a clear Fermi edge. The broad continuum of energy losses in the HREELS spectra, extending up to some hundreds of meV, is due to the excitation of low-frequency plasma oscillations in the metallic surface reconstructed layer.[30] The β-$FeSi_2$ formation is revealed by the shape of the valence band, due to Fe(d)-Si(p) hybrid states. In fact a comparison with the calculated density of states shows very good agreement.[2] The clear loss structure at 50 meV is a further fingerprint of the formation of the semiconducting phase of iron disilicide. It has been shown to correspond to long wavelength surface phonon excitation, also known as Fuchs-Kliewer (FK) surface phonons.[10] The energy of the FK surface modes is closely related to that of the bulk optical phonons in the material.[31] The feature in the loss spectrum is a convolution of several phonon peaks because of the lower resolution of our measurements (FWHM~8 meV) as compared with infrared spectroscopy. By measuring with better resolution, even energy-loss spectra are able to resolve the fine structure of the spectrum.[32]

However, there is a physical reason why in this case the HREELS spectrum of the β-$FeSi_2$ is so poorly resolved. In fact the high intensity background shown by the HREELS spectrum in Fig. 11 after the growth of β-$FeSi_2$ is caused by the presence of a free-carrier accumulation layer at the surface.[33] Low-energy plasma excitations of the free carriers in the vicinity of the surface are responsible for the background intensity, the same as on the metallic (7 × 7) reconstructed silicon surface. If hydrogen adsorbs on the β-$FeSi_2$ surface, then the background in HREELS is mainly removed and the elastic peak width has correspondingly reduced, as shown in Fig. 11. The observed shift of the VBM to higher binding energies in UPS is a further indication that the band bending and therefore the accumulation layer has been removed by hydrogen adsorption. If the sample is now annealed above the temperature at which hydrogen desorbs (550 °C), then both UPS and HREELS typical features related to the accumulation layer at the surface are recovered. The position of the Fermi level relative to the valence band maximum shows that β-$FeSi_2$ is a p-type semiconductor, at least at the surface, and this is in agreement with what is generally reported in the literature. A background hole density at RT in the range of $p = 10^{18}$–10^{19} cm^{-3} is typically measured in epitaxial β-$FeSi_2$ layers on silicon. The presence of acceptorlike states localized near to the surface on the GSMBE-grown β-$FeSi_2$ explains the spectroscopic results of Fig. 11. In fact they pin the Fermi level close to the VBM and induce a hole accumulation layer in the surface region. These states are reproducibly removed from the energy gap by hydrogen treatment of the surface.

A closer insight into the electronic properties of the β-

$FeSi_2$ epitaxial layers grown by GSMBE is achieved by a model calculation of the HREELS spectra. In Fig. 12 the experimental spectra measured on the β-$FeSi_2$/Si(111) heterostructure before (a) and after hydrogen adsorption (b) are reported again (circles) together with a semiclassical model calculation (continuous line) based on the dielectric theory.[34] In this model the loss spectra are calculated by considering the kinematics parameters of the electron scattering (experimental setup) and the dielectric properties of the scattering medium. In particular, the model has been developed for layered structures. It is based on the calculation of an effective dielectric function that depends on the bulk dielectric properties of each layer, after considering the appropriate boundary conditions. The parameters entering the model, concerning the dielectric properties of each layer, are the high-frequency dielectric constant and the Lorentzian oscillators describing the transverse-optical phonons in the material. These data are normally deduced from infrared spectra. This is also the case for β-$FeSi_2$ where phonon parameters have been derived that reproduce the HREELS spectra well, by fitting optical data.[10,32]

It has been shown in Sec. IV B that a metallic γ-$FeSi_2$ layer is stabilized at the interface during the GSMBE on Si(111). At 450 °C growth temperature the layer is quite uniform with a thickness of about 10 Å. This metallic layer is considered in the calculation and even though it is buried at about 400 Å below the surface, its presence also causes a slight broadening of the main structures in the spectra. This can be understood by considering that in the dipole scattering regime the interacting fields have long range character; they penetrate a couple of hundred angstroms into the solid. The dielectric properties of the γ layer are described by means of a free-carrier Drude contribution and the parameters are derived from an optical study performed on a metallic epitaxial pseudomorphic $FeSi_2$ phase grown on Si(111) by MBE.[35] A free-carrier contribution is also considered for the β-$FeSi_2$ layer. The effective mass of the holes in the material is taken as $0.8m_0$, m_0 being the free electron mass.[26] The free-carrier Drude parameters, together with the thickness and sequence of each layer assumed in the sample structures, are listed in Table I. The high intensity background of the spectrum measured after growth [Fig. 12(a)] is well reproduced if a hole accumulation layer at the surface with a thickness of 100 Å is assumed. The removal of this accumulation layer, leaving the other parameters fixed, provides a calculated spectrum in good agreement with the one measured after hydrogen adsorption [Fig. 12(b)]. There is certainly some arbitrariness in the choice of some model parameters. The significant point is that within many possibilities only the assump-

TABLE I. Model parameters for the calculated spectra (continuous line) shown in Figs. 12(a) and 12(b), respectively. Thicknesses and the Drude theory parameters are listed for each layer in the model samples. The assumed layer sequence is shown in the insets of Fig. 12.

	d (Å)	Concentration or ω_p (cm^{-3} or eV)	μ or τ (cm^2/Vs or s)
Fig. 12(a)			
p^+-β-$FeSi_2$	100	$p = 6 \times 10^{20}$	$\mu = 1.8$
β-$FeSi_2$	300	$p = 1.5 \times 10^{18}$	$\mu = 7.5$
γ-$FeSi_2$	10	$\omega_p = 3$	$\tau = 5 \times 10^{-16}$
Si (substrate)		$n = 2 \times 10^{15}$	$\mu = 1500$
Fig. 12(b)			
β-$FeSi_2$	400	$p = 1.5 \times 10^{18}$	$\mu = 1.8$
γ-$FeSi_2$	10	$\omega_p = 3$	$\tau = 5 \times 10^{-16}$
Si (substrate)		$n = 2 \times 10^{15}$	$\mu = 1500$

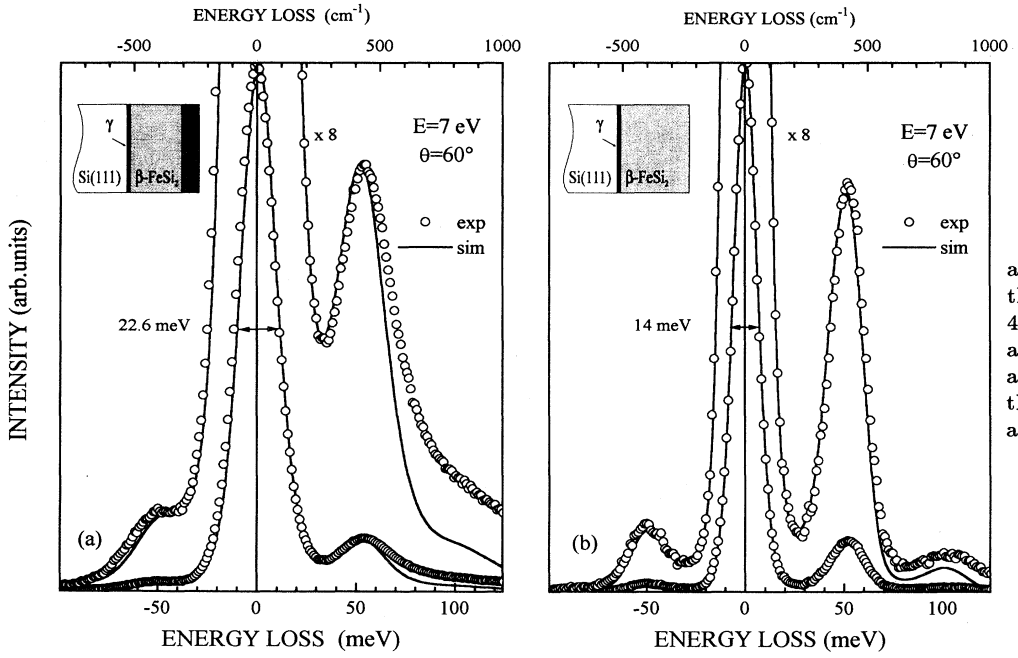

FIG. 12. HREELS spectra as in Fig. 11, measured (a) after the $FeSi_2$ GSMBE on Si(111) at 450 °C and (b) after hydrogen adsorption at RT. The circles are the experimental data and the solid lines are the results of a model calculation (see text).

tion of the surface accumulation layer turns out to give reasonable agreement between experiment and simulation.

In order to further investigate various possibilities for silicide GSMBE growth, the silicon source has been exchanged and Si_2H_6 is considered in the following. From Si homoepitaxy it is known that disilane has a relatively high reactivity compared to silane, which enables higher Si growth rates.[36] The ratio of the Si_2H_6 to SiH_4 sticking coefficient is about 10^3.[37] Since we have seen that the kinetics of the surface reaction plays a major role in determining the growth mode and orientation of β-$FeSi_2$ on silicon, it is expected that Si_2H_6 could provide some more insight into the behavior of this puzzling system.

VI. GROWTH PROCESS WITH Si_2H_6

The GSMBE has been performed in this case on Si(111) substrates. The effect of different partial pressure ratios for the two gas sources has been investigated at first, in analogy to the SiH_4 process (Sec. III). Si:Fe atomic ratio values within the range 0:1–10:1 have been applied. The $Fe(CO)_5$ pressure is fixed and it has been assumed that each Si_2H_6 molecule provides two Si atoms at the surface. The growth temperature is 550 °C and the deposition time is 3 h. A SEM analysis (not reported here) shows different surface morphologies for different Si:Fe ratios. In the lower Si:Fe range, up to 4:1, there results a high roughness of the grown layer indicating a 3D growth of the silicide phase. By increasing the Si-to-Fe gas feed the roughness decreases and in the range 5:1–10:1 quite smooth surfaces are obtained. The same tendency is also reported in a study of the $FeSi_2$ growth on Si(111) performed in comparable experimental conditions.[38]

Rutherford backscattering spectra of two samples grown with Si:Fe ratios of 1:1 and 10:1, respectively, are shown in Fig. 13. The roughness of the sample grown with the lower Si_2H_6 pressure, Fig. 13(a), induces the tail in the Fe signal between 0.9 and 1 MeV energy. For the simulation also shown in full line a layer with a homogeneous thickness of 800 Å and a $FeSi_2$ composition on a silicon substrate are assumed. The RBS and channeling spectra of the sample grown with 10:1 Si:Fe atomic ratio are shown in Fig. 13(b) (filled and open circles, respectively). The minimum channeling yield is 75%. The simulation assumes a homogeneous thickness of 900 Å and a $Fe_{0.85}Si_2$ composition.

Correspondingly also different electronic properties are measured for the two different Si:Fe ratio ranges. For the lower Si:Fe values, both UPS and HREELS show the typical features of β-$FeSi_2$, like the ones shown in Fig. 11 (center). Due to the bad surface morphology the intensity of the elastic peak in HREELS is much reduced as compared to the SiH_4 grown samples. LEED patterns correspond to the β-$FeSi_2(100)\|Si(111)$ epitaxy. The spectra measured on a sample grown with a Si:Fe ratio of 10:1 are presented in Fig. 14. The main structure at the top of the valence band has narrowed in comparison to the silicide spectra in Fig. 11. The density of occupied states shows a clear Fermi edge, indicating the formation of a metallic phase. This is also confirmed by the struc-

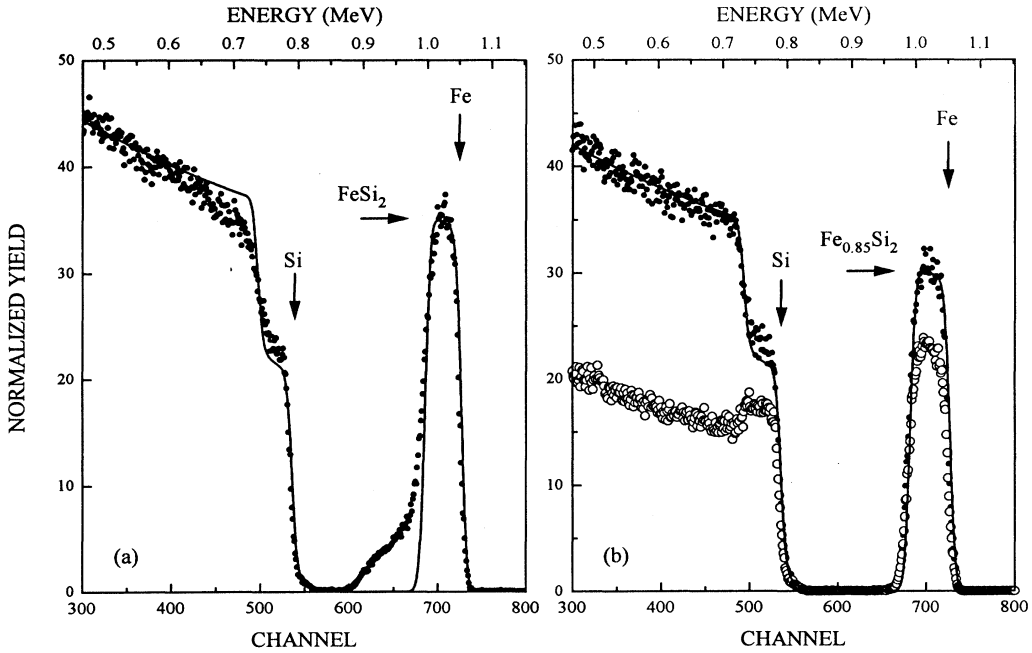

FIG. 13. RBS random (dots) and channeling (circles) spectra of samples grown by GSMBE with Si_2H_6 at 550 °C. The solid lines are the result of a simulation (see text). The deposition time is 3 h. The Si:Fe ratio is (a) 1:1 and (b) 10:1

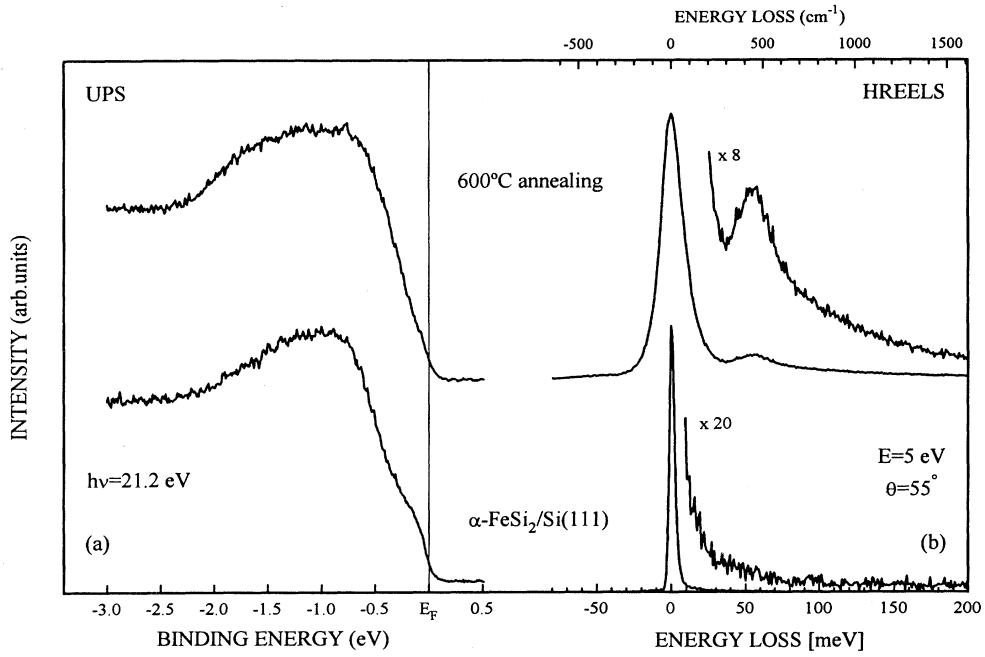

FIG. 14. UPS and HREELS spectra measured at room temperature, from the bottom to the top, after the GSMBE of $FeSi_2$ at 550 °C (d = 900 Å) with a Si:Fe atomic ratio of 10:1 and after 30 min annealing at 600 °C. (a) Ultraviolet photoemission spectra. Photon energy is 21.2 eV, the Fermi level position is indicated by a vertical line at zero binding energy. (b) High-resolution electron-energy-loss spectra measured with a primary beam energy of 5 eV under specular reflection with 55° angle of incidence.

tureless HREELS spectrum with a narrow elastic peak (FWHM=4 meV) (Ref. 39) that reveals the presence of a metallic layer of some hundred angstroms of thickness. A very thin metallic layer at the surface can be excluded, because no broadening of the elastic peak is observed due to 2D plasmon excitations. LEED patterns show a (2×2) reconstruction at the surface.

Figure 15 shows a cross-section TEM image of a layer grown at 500 °C for 3 h with a Si:Fe atomic ratio of 5:1. The thickness of the overlayer is about 1200 Å and its diffraction pattern is shown in the inset. It corresponds to the growth of α-$FeSi_2$ on Si(111) with the epitaxial relation α-$FeSi_2(112)\|Si(111)$.

The metallic α phase of $FeSi_2$ is the bulk phase that is stable above 937 °C. It has tetragonal structure with $a = b = 2.69$ Å and $c = 5.134$ Å and deviates from the stoichiometric composition by about 13% Fe vacancies. The formation of buried α-$FeSi_2$ layers by iron implantation and subsequent annealing below the phase transition temperature of 937 °C has been demonstrated to be a successful technique to fabricate buried semiconducting β-$FeSi_2$ layers.[40,41] As already mentioned in Sec. IV, thin epitaxial α-$FeSi_2$ layers have been stabilized even at low temperatures on Si(111). In fact, the lattice mismatch is quite favorable if one considers a supercell for α-$FeSi_2$ with $a' = b' = 2a = 5.38$ Å and $c' = c = 5.134$ Å compared to $a = 5.43$ Å for silicon. The (111) planes of this quasicubic supercell grow parallel to the Si(111) surface, according to the observed epitaxial relations. The inferred growth of the α phase in the presence of a higher Si:Fe feed ratio is also supported by the RBS analysis. The composition of the disilicide layer turns out to be not stoichiometric and the simulation gives $Fe_{0.85}Si_2$ that is in agreement with Fe vacancy concentrations generally found in α-$FeSi_2$.

In the spectroscopic *in situ* investigation (Fig. 14) the presence of a Fermi edge in UPS and of the free electron background in HREELS clearly reveal the formation of a metallic phase. The observed (2×2) surface reconstruction in LEED has been explained in the literature in terms of a Si terminated layer on the epitaxial silicide.[42,43] The α-$FeSi_2$ can be gradually transformed to the semiconducting β-$FeSi_2$ by annealing at 600 °C. The spectra at the top of Fig. 14 are measured after 30 min annealing at 600 °C. In the HREELS spectrum the typical phonon loss, fingerprint of the β phase formation, appears on a high loss background; correspondingly the valence band changes its shape towards the one measured on the semiconducting β phase (Fig. 11). However, the β-$FeSi_2$ nucleation is not complete after this annealing step as revealed by the intermediate shape of the valence

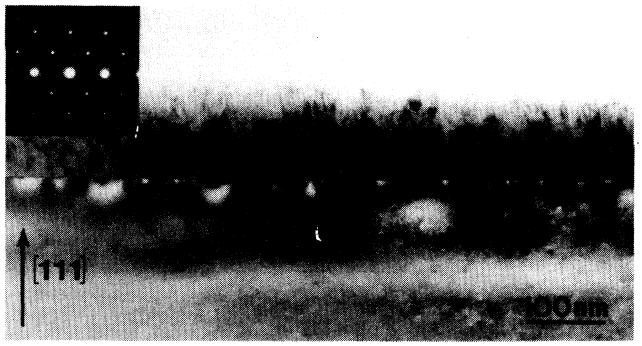

FIG. 15. Cross-section TEM image of a sample grown at 550 °C with a Si:Fe atomic ratio of 5:1. The inset shows the diffraction pattern of the overlayer.

band. Plan-view TEM analysis on such samples shows β-$FeSi_2$ grains embedded in the α-$FeSi_2$ matrix.

In comparison with the silane process, the β-$FeSi_2$ GSMBE with disilane does not show any improvement. In the parameter range where the β phase grows, a higher roughness is observed. The orientation of the epitaxial grains is the same, indicating a very similar mechanism for the growth in the two cases. The morphological quality of the β-$FeSi_2$ layer therefore seems to be determined by the growth rate, which in the Si_2H_6 process is increased, even though its absolute value ($\leq$ 10 Å/min) remains low as compared with other systems. In contrast to what is claimed in Ref. 24 we do not have any evidence of such a breakthrough in the quality of the β-$FeSi_2$ layers formed by long annealing of the as-grown α layers. The surface looks indeed smoother, as observed by SEM, but the optical and electrical properties that will be discussed in the next section remain practically the same.

An interesting point is the comparison of the two growth processes performed in this study in the temperature range 500–550 °C. The use of Si_2H_6 provides a higher efficiency of the silicon source as compared with SiH_4 and therefore the Si-rich environment at the growing surface induces the formation of the epitaxial, nonstoichiometric α-$FeSi_2$. Apparently, such a Si-rich environment has not been realized in the case of SiH_4 and therefore the interface-stabilized epitaxial phase turns out to be the stoichiometric γ-$FeSi_2$. Once the kinetics has induced the growth of the specific interface-stabilized $FeSi_2$ phase, it is experimentally seen that the α-$FeSi_2$ can be stabilized in relatively thick layers, of the order of 1000 Å, whereas the γ-$FeSi_2$ interface layers have never been seen to be thicker than about 10 Å. This observation can be qualitatively understood by the fact that the α phase appears as equilibrium phase for the $FeSi_2$ system, even though at high temperatures (above 937 °C), but this is not the case for the γ-phase. Now, taking into account the similar lattice mismatches and interfaces between Si(111) and the two epitaxial phases, i.e., a similar energy gain through interface stabilization, the observed behavior seems reasonable. These conclusions are, of course, speculative, but supported by the experimental results; they might be helpful in shedding some light on the manifold aspects of the growth of $FeSi_2$/Si heterostructures.

In order to clarify the potential role that might be played by β-$FeSi_2$ in the field of optoelectronics and microelectronics optical and electrical characterization of the grown heterostructures is needed. In the following, results on samples grown by GSMBE with Si_2H_6 are reported.

VII. OPTICAL AND ELECTRICAL PROPERTIES

An important question to be answered for β-$FeSi_2$ is the nature of its energy gap. First spectral transmission and reflection experiments on polycrystalline β-$FeSi_2$ thin layers reported an absolute direct gap of 0.89 eV at room temperature.[44] Band structure calculations show a minimum indirect gap very close in energy to the direct gap at Γ.[26] A recent absorption experiment on polycrystalline samples confirmed the theoretical prediction of an indirect gap material with an absolute gap energy a few tens of meV lower than the direct one at 0.9 eV (80 K).[7] Other absorption experiments lead to a similar conclusion,[8] but it must be pointed out that a significant defect absorption below the fundamental edge makes the identification of an indirect gap lower in energy than the direct one uncertain.[1,2] However, it should be mentioned that our samples do not show any photoluminescence signal at the band gap energy and in our opinion no clear photoluminescence (PL) signal from β-$FeSi_2$ has been reported up to now in the literature. This observation agrees both with an indirect gap material and with a high density of nonradiative centers in the gap.

Figure 16 shows the optical absorption coefficient α in the energy range from 0.5 to 1.5 eV for a β-$FeSi_2$/Si(111) heterostructure. The optical absorption is determined using photothermal deflection spectroscopy (PDS). Absorption spectra of Ge, Si, and GaAs close to their fundamental gap are also shown for comparison.[45] A clear absorption edge for the β-$FeSi_2$ is measured at $\sim$ 0.87 eV. However, the comparison with the other materials clearly shows the defect absorption measured at energies below the edge energy. Its intensity slightly decreases with in-

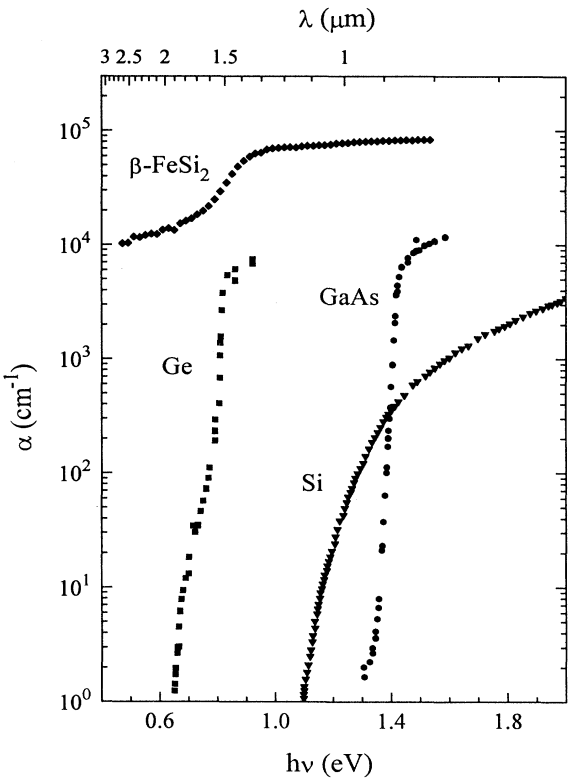

FIG. 16. Absorption coefficient α measured by photothermal deflection spectroscopy (PDS) on a β-$FeSi_2$/Si(111) heterostructure. The silicide thickness is 800 Å. The absorption spectra of other semiconductor materials are reported for comparison (Ref. 45.)

creasing growth temperature in the GSMBE process.[2]

The absolute value of the absorption coefficient is estimated by considering the saturation intensity value above the edge and the film thickness. As compared to other material, β-$FeSi_2$ shows a high absorption that can be related to the partial d character of the density of states at the band edge.[26] In view of applications, e.g., in solar cells and photodetectors, this high absorption coefficient might be of interest.

Figure 17 shows the results of electrical measurements on a β-$FeSi_2$/Si(111) heterostructure by Hall-effect measurements. The thickness of the silicide layer is about 1500 Å; the Si(111) substrate is n-type with a resistivity of 5000 Ω cm.

The resistivity ρ [Fig. 17(a)] and the absolute value of the Hall constant [Fig. 17(b)] are shown in the temperature range from 30 K up to room temperature. The resistivity decreases with increasing temperature and its RT value is about 0.3 Ω cm. The Hall constant is positive at low temperatures up to 200 K where a sign change is observed. No significant deviation from a linear dependence of the Hall voltage on the magnetic field is measured at low temperature. The change in the sign of the carriers from p to n at about 200 K by increasing temperature is characteristic for our β-$FeSi_2$ layers, when grown on an n-type substrate, independent of the layer thickness. For silicide layers grown on p-type substrates, the Hall constant as a function of temperature has a varying behavior, but it remains positive in the whole investigated temperature range. These results suggest an influence of the substrate above 200 K; therefore RT values for the mobility and carrier concentration in the β-$FeSi_2$ layers are difficult to extract. In the low temperature range the conduction is p type, as generally measured for semiconducting iron disilicide. Typical values of the mobility and the carrier concentration at 77 K in samples grown on n-type Si(111) substrates are $\mu \sim 2$ cm^2/V s and $p \sim 2 \times 10^{18}$ cm^{-3}.

The reported results of the optical and electrical characterization of β-$FeSi_2$/Si heterostructures together with the structural properties discussed in the previous sections indicate that the quality of the material needs to be improved, if one thinks of optoelectronics and microelectronics applications. In a recent study of the Hall effect in β-$FeSi_2$ needlelike single crystals, values up to 1200 cm^2/V s for the mobility of holes at low temperature are claimed.[46] However, many different epitaxial growth methods have been employed so far, but in our opinion no significant breakthrough in the quality of β-$FeSi_2$ has been demonstrated yet. A way of improving the material quality and possibly confirming the promising results recently obtained on single crystals[46] might be given by limiting the lateral size of the β-$FeSi_2$ layers grown. The possibility of growing microstructures is given by the selective growth on a SiO_2 patterned substrate; this is achieved in a relatively simple way by GSMBE processes. In Fig. 18 a SEM picture is shown of a sample grown at 500 °C with Si_2H_6 on a Si(001) patterned substrate. It can be recognized that the β-$FeSi_2$ only grows on the Si bare areas but not on the silicon oxide. The lateral dimension of the β-$FeSi_2$ dots grown is 0.5×0.5 μm^2, which is of the same order of the lateral dimensions of a single crystal β-$FeSi_2$ grain (Sec. IV).

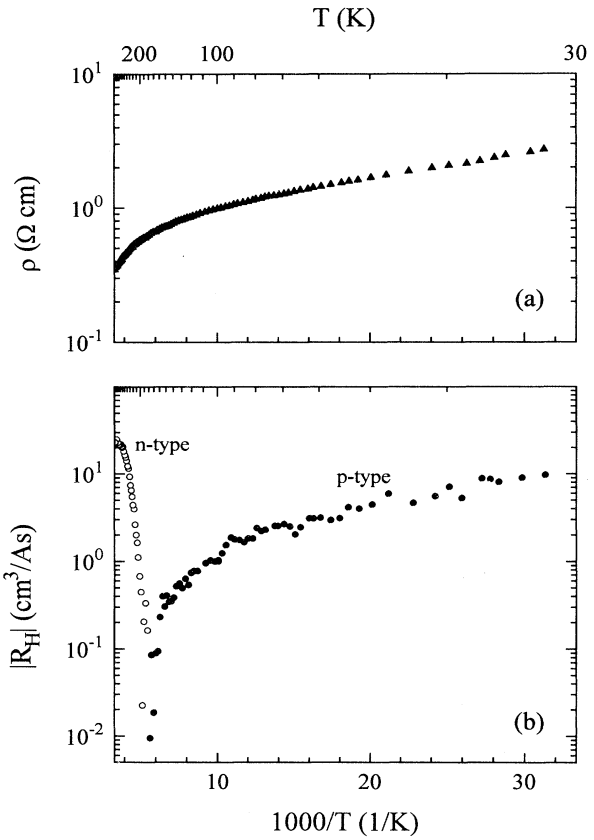

FIG. 17. Electrical resitivity (a) and Hall coefficient (b) measured on a β-$FeSi_2$/Si(111) heterostructure as a function of temperature. The silicon source is Si_2H_6, Si:Fe ratio is 4:1, the growth temperature is 500 °C. The thickness of the silicide layer is about 1500 Å.

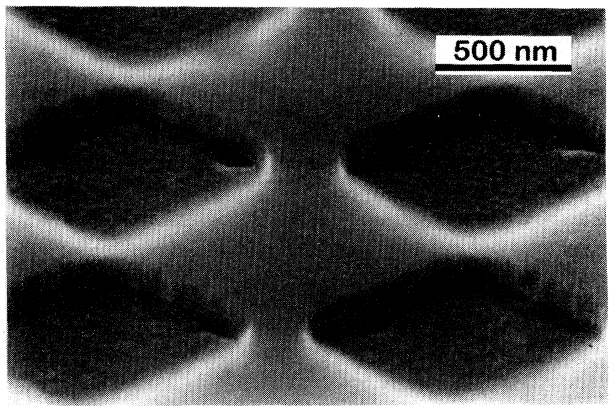

FIG. 18. SEM picture of β-$FeSi_2$ grown by GSMBE on a SiO_2 patterned Si(001) substrate. The silicon source is Si_2H_6, Si:Fe ratio is 4:1, and the growth temperature is 500 °C. The silicide grows selectively in the bare silicon area with size 500×500 nm^2.

The growth and characterization of such microstructures certainly is an interesting field for further investigations on semiconducting β-$FeSi_2$.

VIII. CONCLUSIONS

β-$FeSi_2$/Si heterostructures grown by gas-source MBE have been characterized by means of several *in situ* and *ex situ* techniques. The comparison of two different GSMBE processes, differing by the use of SiH_4 or Si_2H_6, has shown that surface kinetics plays a dominant role in the silicide phase formation. The relevant temperature range for the growth is 450–550 °C; at higher temperatures the layers are very rough, with rough interfaces to the substrate. On Si(111) metallic $FeSi_2$ phases are stabilized at the interface in the lower growth temperature range. The use of SiH_4 induces the formation of a very thin cubic γ-$FeSi_2$ that remains stabilized at the interface during subsequent growth of semiconducting β-$FeSi_2$. If the silicon supply at the surface is increased by using Si_2H_6, the tetragonal nonstoichiometric α-$FeSi_2$ is stabilized by the interface and corresponding layers grow up to several hundred angstroms of thickness. Such α-$FeSi_2$ layers can be transformed into the stable semiconducting β-$FeSi_2$ phase by annealing above 600 °C. The lower symmetry of β-$FeSi_2$ in comparison with the relevant silicon surfaces always induces the presence of azimuthal rotated domains. The optical and electrical properties of the heterostructures grown show that the possibility of optoelectronic applications remains speculative. The fabrication of micro- and nanostructures by means of selective growth on SiO_2 patterned substrates might represent an interesting field to improve the material quality.

ACKNOWLEDGMENTS

The authors thank G. Landmesser for his help in part of the experiments. We are grateful to K. Schmidt for the RBS measurements, to R. Carius and J. Klomfaß for the PDS characterization, and to St. Teichert for the collaboration in part of the electrical characterization.

* Permanent address: Dipartimento di Fisica, Università di Modena, via Campi 213/A, I-41100 Modena, Italy.

[1] H. von Känel, U. Kafader, P. Sutter, N. Onda, H. Sirringhaus, E. Müller, U. Kroll, C. Schwarz, and S. Goncalves-Conto, in *Silicides, Germanides, and Their Interfaces*, edited by R. W. Fathauer, S. Mantl, L. Schowalter, and K. N. Tu, MRS Symposia Proceedings No. 320 (Materials Research Society, Pittsburgh, 1994), p. 73.

[2] A. Rizzi, in *Formation of Semiconductor Interfaces*, edited by B. Lengeler, H. Lüth, W. Mönch, and J. Pollmann (World Scientific, Singapore, 1994), p. 439.

[3] J. Chevrier, J. Y. Natoli, I. Berbezier, A. Ronda, and J. Derrien, Solid State Phenom. **32-33**, 39 (1993).

[4] H. von Känel, K. A. Mäder, E. Müller, N. Onda, and H. Sirringhaus, Phys. Rev. B **45**, 13 807 (1992).

[5] H. Sirringhaus, N. Onda, E. Müller-Gubler, P. Müller, R. Stalder, and H. von Känel, Phys. Rev. B **47**, 10 567 (1993).

[6] Le Thanh Vinh, J. Chevrier, and J. Derrien, Phys. Rev. B **46**, 15 946 (1992).

[7] C. Giannini, S. Lagomarsino, F. Scarinci, and P. Castrucci, Phys. Rev. B **45**, 8822 (1992).

[8] K. Radermacher, O. Skeide, R. Carius, J. Klomfaß, and S. Mantl, in *Silicides, Germanides, and Their Interfaces* (Ref. 1), p. 115.

[9] B. N. E. Rösen, D. Freundt, Ch. Dieker, D. Gerthsen, A. Rizzi, R. Carius, and H. Lüth, in *Silicides, Germanides, and Their Interfaces* (Ref. 1), p. 139.

[10] A. Rizzi, H. Moritz, and H. Lüth, J. Vac. Sci. Technol. A **9**, 912 (1991).

[11] F. Hirose, M. Suemitsu, and N. Miyamoto, Jpn. J. Appl. Phys. **29**, L1881 (1990).

[12] J. H. Comfort and R. Reif, J. Electrochem. Soc. **136**, 2386 (1989).

[13] S. M. Gates and S. K. Kulkarni, Appl. Phys. Lett. **58**, 2963 (1991).

[14] R. B. Jackman and J. S. Foord, Surf. Sci. **209**, 151 (1989).

[15] A. F. Holleman and E. Wiberg, *Lehrbuch der Anorganischen Chemie* (de Gruyter, Berlin, 1976), p. 520.

[16] P. Y. Dusausoy, J. Protas, R. Wandji, and B. Roques, Acta Crystallogr., Sect. B **27**, 1209 (1971).

[17] K. M. Geib, J. E. Mahan, R. G. Long, M. Nathan, and G. Bai, J. Appl. Phys. **70**, 1730 (1991).

[18] D. R. Peale, R. Haight, and J. Ott, Appl. Phys. Lett. **62**, 1402 (1993).

[19] N. Cherief, C. D'Anterroches, R. C. Cinti, T. A. Nguyen Tan, and J. Derrien, Appl. Phys. Lett., **55**, 1671 (1989).

[20] D. Gerthsen, H. Ch. Schäfer, B. Rösen, A. Rizzi, H. Moritz, and H. Lüth, in *Microscopy of Semiconducting Materials 1993*, Proceedings of the Royal Microscopical Society Conference, edited by A. G. Cullis, A. E. Staton-Bevan, and J. L. Hutchison, IOP Conf. Proc. No. 134 (Institute of Physics and Physical Society, London, 1993), p. 185.

[21] J. Chevrier, P. Stocker, Le Than Vinh, J. M. Gay, and J. Derrien, Europhys. Lett. **22**, 449 (1993).

[22] N. Jedrecy, A. Waldhauer, M. Sauvage-Simkin, R. Pinchaux, and Y. Zheng, Phys. Rev. B **49**, 4725 (1994).

[23] F. Sirotti, M. De Santis, Xiaofeng Jin, and G. Rossi, Phys. Rev. B **49**, 11134 (1994).

[24] J. Y. Natoli, I. Berbezier, and J. Derrien, Appl. Phys. Lett. **65**, 1439 (1994).

[25] H. Ch. Schäfer, B. Rösen, H. Moritz, A. Rizzi, B. Lengeler, and H. Lüth, Appl. Phys. Lett. **62**, 2271 (1993).

[26] N. E. Christensen, Phys. Rev. B **42**, 7148 (1990).

[27] H. von Känel, N. Onda, H. Sirringhaus, E. Müller-Gubler, S. Goncalves-Conto, and C. Schwarz, Appl. Surf. Sci. **70-71**, 559 (1993).

[28] K. Mäder, H. von Känel, and A. Baldereschi, Phys. Rev. B **48**, 4364 (1993).

[29] L. Miglio and G. Malegori, in *Silicides, Germanides, and Their Interfaces* (Ref. 1), p. 109.

[30] B. N. J. Persson and J. E. Demuth, Phys. Rev. B **30**, 5968 (1984).

[31] G. Guizzetti, F. Marabelli, M. Patrini, Y. Mo, N. Onda, and H. von Känel, in *Silicides, Germanides, and Their Interfaces* (Ref. 1), p. 127.
[32] Ch. Stuhlmann, J. Schmidt, and H. Ibach, J. Appl. Phys. **72**, 5905 (1992).
[33] B. N. E. Rösen, H. Ch. Schäfer, Ch. Dieker, H. Lüth, A. Rizzi, and D. Gerthsen, J. Vac. Sci. Technol. B **11**, 1407 (1993).
[34] Ph. Lambin, J. P. Vigneron, and A. A. Lucas, Comput. Phys. Commun. **60**, 351 (1990), and reference quoted therein.
[35] G. Guizzetti, F. Marabelli, N. Onda, and H. von Känel, Solid State Commun. **86**, 217 (1993).
[36] H. Hirayama, T. Tatsumi, A. Ogura, and N. Aizaki, Appl. Phys. Lett. **51**, 2213 (1987); **52**, 1484 (1988).
[37] S. M. Gates, J. Cryst. Growth **120**, 269 (1992).
[38] T. E. Crumbaker, J. Y. Natoli, I. Berbezier, and J. Derrien, J. Cryst. Growth **127**, 158 (1993).
[39] A new HREEL spectrometer has been built in and since then the intrinsic resolution of the HREEL spectra has been lowered down to FWHM=3 meV. The EELS-90 spectrometer has been developed in the group of Professor H. Ibach at the Forschungszentrum Jülich; for more information refer to H. Ibach, *Electron Energy Loss Spectrometers*, edited by P. W. Hawkes, Springer Series in Optical Sciences Vol. 63 (Springer, Berlin, 1991).
[40] D. J. Oostra, D. E. W. Vandenhoudt, C. W. T. Bulle-Lieuwma, and E. P. Naburgh, Appl. Phys. Lett. **59**, 1737 (1991).
[41] K. Radermacher, S. Mantl, Ch. Dieker, and H. Lüth, Appl. Phys. Lett. **59**, 2145 (1991).
[42] A. L. Vasquez de Parga, J. de la Figuera, C. Ocal, and R. Miranda, Europhys. Lett. **18**, 595 (1992).
[43] N. Jedrecy, Y. Zheng, A. Waldhauer, M. Sauvage-Simkin, and R. Pinchaux, Phys. Rev. B **48**, 8801 (1993), and references quoted therein.
[44] M. C. Bost and J. E. Mahan, J. Appl. Phys. **58**, 2696 (1985); **64**, 2034 (1988).
[45] *Semiconductors, Physics of Group IV Elements and III-V Compounds*, edited by O. Madelung, M. Schulz, and H. Weiss, Landolt-Börnstein, New Series, Group III, Vol. 17, Pt. a (Springer, Berlin, 1982).
[46] E. Arushanov, Ch. Kloc, H. Hohl, and E. Bucher, J. Appl. Phys. **75**, 5106 (1994).

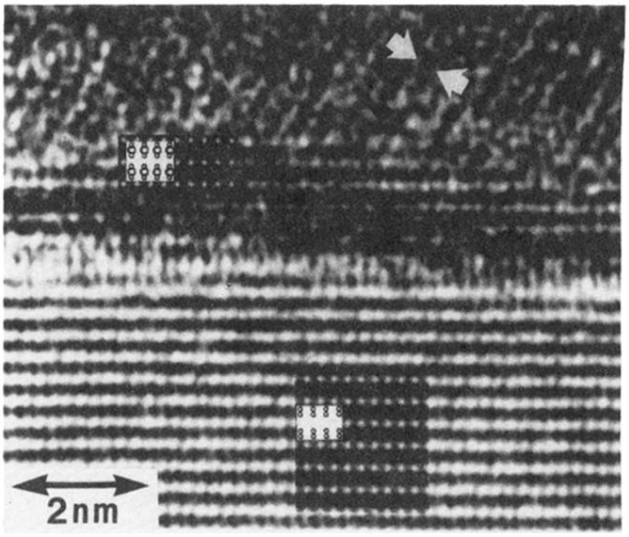

FIG. 10. High-resolution cross-section image with a Si⟨112⟩ zone axis oriented parallel to the electron beam. The interface region is shown with a thin γ-$FeSi_2$ layer [1–6 Si(111) layers] located between the substrate and the β-$FeSi_2$. The insets show simulations of the γ-$FeSi_2$ and the Si based on structural models also inserted in the figure (large circles Fe, small circles Si).

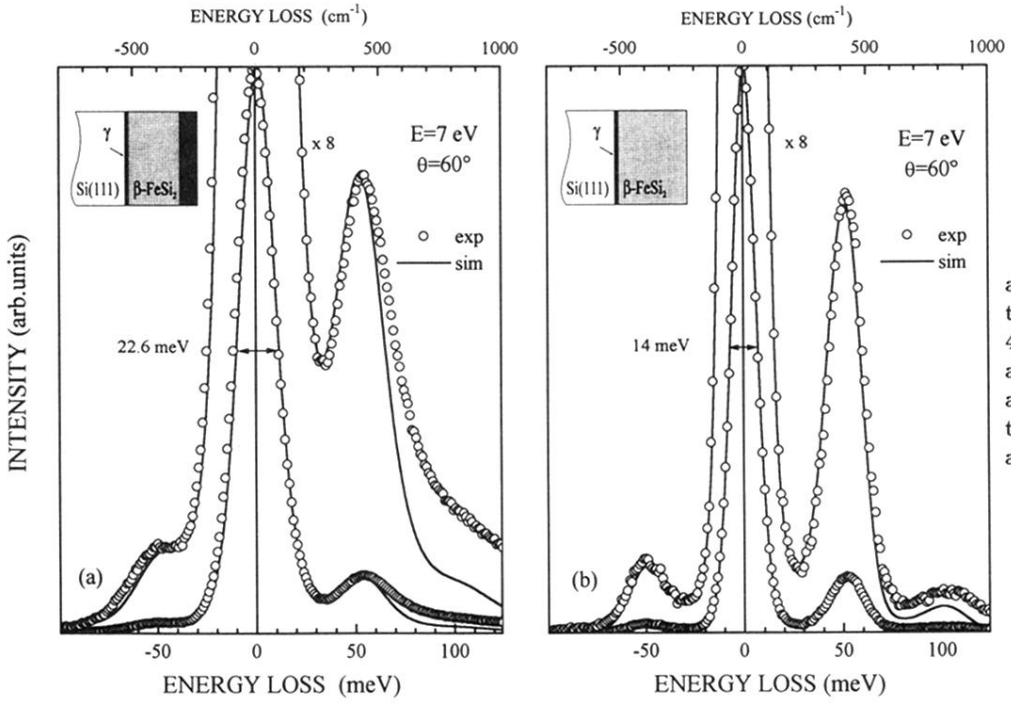

FIG. 12. HREELS spectra as in Fig. 11, measured (a) after the $FeSi_2$ GSMBE on Si(111) at 450 °C and (b) after hydrogen adsorption at RT. The circles are the experimental data and the solid lines are the results of a model calculation (see text).

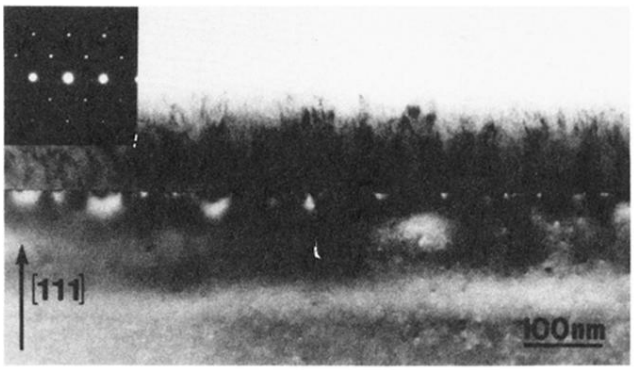

FIG. 15. Cross-section TEM image of a sample grown at 550 °C with a Si:Fe atomic ratio of 5:1. The inset shows the diffraction pattern of the overlayer.

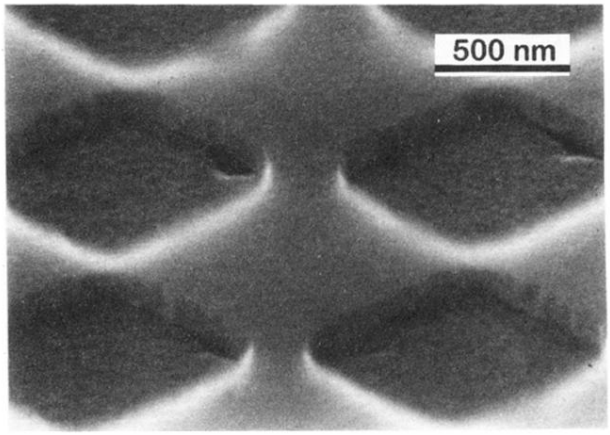

FIG. 18. SEM picture of β-$FeSi_2$ grown by GSMBE on a SiO_2 patterned Si(001) substrate. The silicon source is Si_2H_6, Si:Fe ratio is 4:1, and the growth temperature is 500 °C. The silicide grows selectively in the bare silicon area with size 500×500 nm^2.

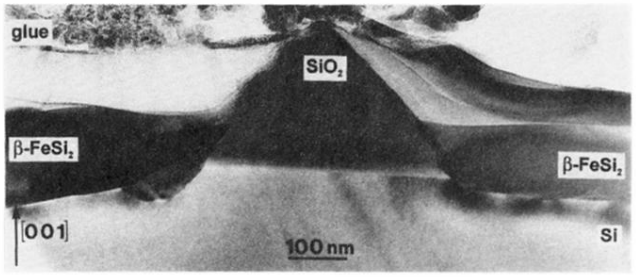

FIG. 2. Cross-section TEM image showing the growth of β-$FeSi_2$ on a SiO_2 patterned Si(001) substrate. Growth temperature is 700 °C.

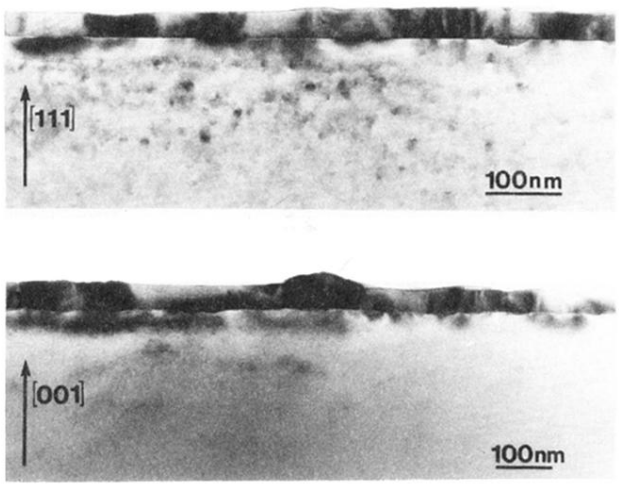

FIG. 3. Cross-section TEM images of β-$FeSi_2$ layers grown on Si(111) (top) and Si(001) (bottom). Growth temperature is 550 °C and growth time 3 h.

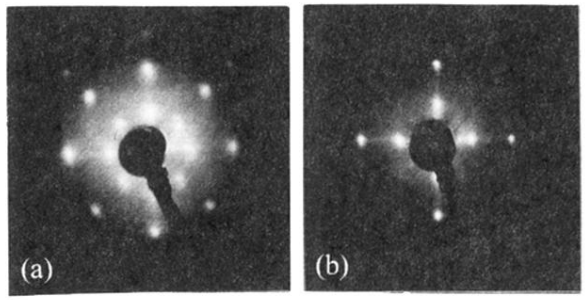

FIG. 4. 63 eV LEED pattern of epitaxial β-$FeSi_2$ grown on Si(001) at (a) 550 °C (d = 360 Å) and (b) 700 °C (d = 900 Å).

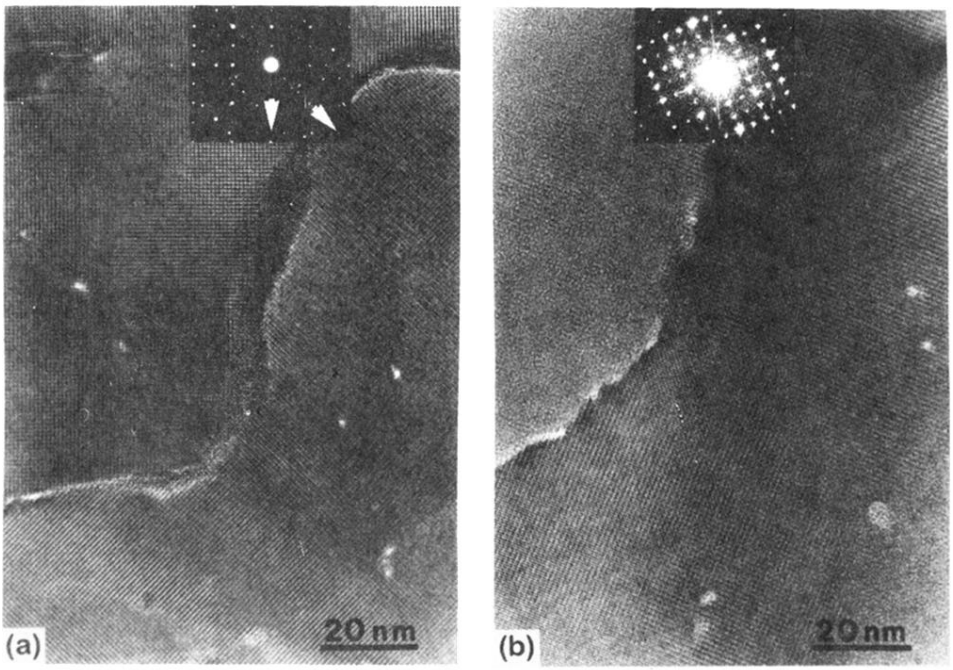

FIG. 6. HRTEM plan-view picture of β-$FeSi_2$(100) grown on Si(001) showing the boundary region between two epitaxial grains. (a) Grain boundary region of two domains rotated by 45°. (b) Grain boundary region of two domains that are only slightly tilted against each other. The lattice fringe resolution is reduced due to the tilt. The optical diffractograms of the boundary areas are inserted in the images.

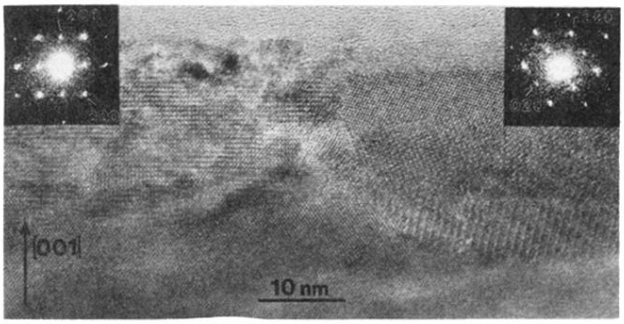

FIG. 7. Cross-section HRTEM image of two differently oriented grains (left and right) with the insets showing the optical diffractograms of the two regions. β-$FeSi_2$ was grown by GSMBE at 550 °C.

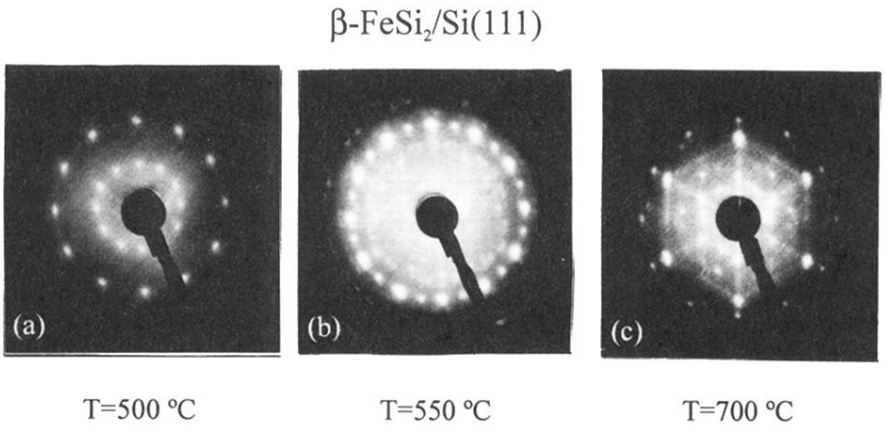

FIG. 8. LEED pattern of epitaxial β-$FeSi_2$ grown on Si(111) at (a) 500 °C (E = 46 eV, d = 500 Å), (b) 550 °C (E = 43 eV, d = 100 Å), and (c) 700 °C (E = 46 eV, d = 800 Å).